

ALINet: Partial-Shape Agnostic Alignment via Unsupervised Learning

RANA HANOCKA, Tel Aviv University

NOA FISH, Tel Aviv University

ZHENHUA WANG, Hebrew University

RAJA GIRYES, Tel Aviv University

SHACHAR FLEISHMAN, Intel Corporation

DANIEL COHEN-OR, Tel Aviv University

The process of aligning a pair of shapes is a fundamental operation in computer graphics. Traditional approaches rely heavily on matching corresponding points or features to guide the alignment, a paradigm that falters when significant shape portions are missing. These techniques generally do not incorporate prior knowledge about expected shape characteristics, which can help compensate for any misleading cues left by inaccuracies exhibited in the input shapes. We present an approach based on a deep neural network, leveraging shape datasets to learn a *shape-aware* prior for source-to-target alignment that is robust to shape incompleteness. In the absence of ground truth alignments for supervision, we train a network on the task of shape alignment using incomplete shapes generated from full shapes for self-supervision. Our network, called *ALINet*, is trained to warp complete source shapes to incomplete targets, as if the target shapes were complete, thus essentially rendering the alignment *partial-shape agnostic*. We aim for the network to develop specialized expertise over the common characteristics of the shapes in each dataset, thereby achieving a higher-level understanding of the expected shape space to which a local approach would be oblivious. We constrain *ALINet* through an anisotropic total variation identity regularization to promote piecewise smooth deformation fields, facilitating both partial-shape agnosticism and post-deformation applications. We demonstrate that *ALINet* learns to align geometrically distinct shapes, and is able to infer plausible mappings even when the target shape is significantly incomplete. We show that our network learns the common expected characteristics of shape collections, without over-fitting or memorization, enabling it to produce plausible deformations on unseen data during test time.

1 INTRODUCTION

Shape registration is a fundamental problem in computer graphics and computer vision, with diverse applications ranging from object recognition and scene understanding to texture or attribute transfer and synthesis. Classic approaches draw from a predefined family of transformations to obtain a warp that optimizes the registration between two shapes. While successful in straight-forward scenarios, the limitations of this paradigm are revealed as we seek to match increasingly distinct shapes differing in geometry and topology. Given such differences, restricting the pool of allowed transformations (e.g., affine transformations) is often insufficient, requiring higher-order deformations (e.g., free-form deformation). The problem becomes even more challenging when the shape is partial, for example due to missing data or occlusions.

Typically, the desired transformation between two shapes is obtained by solving a set of constraints defined by sparsely matching corresponding points or features on the shapes in question. Point matching necessitates a modicum of geometric resemblance between point neighborhoods, which is not always at hand under moderate to large differences. To alleviate this difficulty, features or

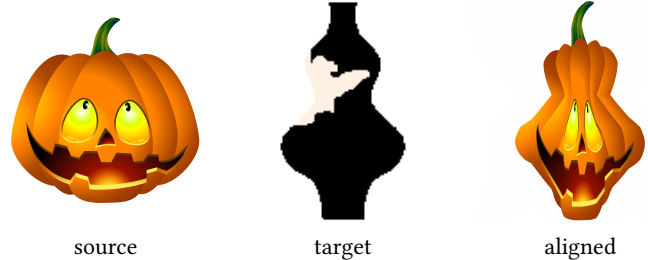


Fig. 1. ALINet aligns a *pumpkin* to a partial *vase* (missing part visualized in pink), resulting in a *vase-like pumpkin* (aligned).

descriptors are computed and matched instead. However, designing descriptors to be sensitive to interesting aspects of the shape yet robust to less significant variations, as well as to a wide range of shape types, is a daunting, and at times even intractable, task. As a further complication, when the shape is incomplete, the process of feature matching becomes even more ambiguous and prone to errors. Moreover, traditional methods locally optimize the alignment between a pair of shapes without incorporating prior knowledge about their geometric and semantic identity. This information may provide invaluable cues as to the expected outcome, and guide the alignment both generally, as well as in and around the missing regions, such that geometric features typical to the relevant class of objects are preserved.

Inspired by the recent irrefutable success of deep learning methods applied to various computer vision problems, we propose a data-driven learning approach to address the problem of partial shape alignment. Instead of providing a local solution, we opt to leverage the ever-growing availability of large collections of shapes to learn a data-aware global warping model. Many of these shape collections are consistently pre-oriented (or can be oriented e.g., by employing hierarchical alignment [Chang et al. 2015]), and contain a rich variety of examples that collectively form a comprehensive guide capturing the characteristic attributes of the set, such as common geometry, topology, and even semantic high-level features such as part existence. We arrange this data into random pairs of source and target shapes, and train a convolutional neural network (CNN) to learn the mapping between input source and target shapes. We employ grid-based free-form deformation (FFD [Sederberg and Parry 1986]), a new type of high order spatial transformer (STN) [Jaderberg et al. 2015], which is simple yet expressive enough to support a wide range of alignments. Unlike STN, we deliberately learn to align a source shape to an incomplete target, as though it were complete

(e.g., Figure 1). As shown in Figure 2, we are able to warp a model’s texture to different partial target shapes, even when the target is missing more than 50% of the original shape (all shapes are from the test set and therefore unseen during training). Furthermore, we are able to faithfully predict the scale (even in ambiguous scenarios such as target B) and correctly reconstruct symmetries of missing parts (target A).

Our approach is completely unsupervised, in that we do not supply any ground-truth warps that the network is expected to reproduce. Instead, the network is trained with a shape alignment loss, comparing the overlap between the warped source and the expected (complete) target, acting as a proxy for learning the desired underlying FFD parameters. As the network is trained, it essentially familiarizes itself with the common characteristics of the shapes in each dataset, allowing it to form a higher-level understanding of the expected shape space to which a local approach would be oblivious. As such, our network is able to deal with incomplete, partial shapes, inferring plausible mappings in the missing regions by computing a *class-aware* alignment. By training to warp complete source shapes to incomplete targets, as if the target shapes were complete, our network learns to be *partial-shape agnostic*: unaffected by missing shape parts.

Due to the unsupervised nature of our training, in its simplest form, the model is given free reign in terms of the warp fields it is allowed to output, as long as the end result is deemed appropriate. Specifically, there are many vastly different FFDs that, when applied on *binary shapes*, yield the same shape alignment cost. Such a behavior is undesirable when the warp field is needed for further processing; thus, to ensure the quality and dependability of our warps, we introduce a key addition to regulate the space of possible transformations. This addition encourages piecewise smooth warp fields by penalizing the total variation of the deviation of the warp field from the identity. By tuning the weighted contribution of this regularization component to the overall score, we are better able to control the degree of freedom given to the network for warp computation. We show that this step benefits not only post-deformation processes, but also partial agnosticism.

2 RELATED WORKS

Common shape registration methods estimate a transformation from a pre-determined class of transformations, by evaluating the overall shape-to-shape alignment. The classic Iterative Closest Point (ICP) method [Besl and McKay 1992] uses nearest neighbor correspondences to refine the transformation, which minimizes the mismatch between the source and target points. Follow-up works propose numerous variants of ICP involving modifying the constraints defined to compute the transformation [Rusinkiewicz and Levoy 2001]. Other methods assume a global probabilistic approach [Jian and Vemuri 2011; Myronenko and Song 2010; Tsin and Kanade 2004], or more recently incorporate local structure to further improve results [Ma et al. 2014, 2016]. To handle partial shapes, these approaches must explicitly incorporate outlier rejection and intelligently select a subset of appropriate points, a challenging task in and of itself.

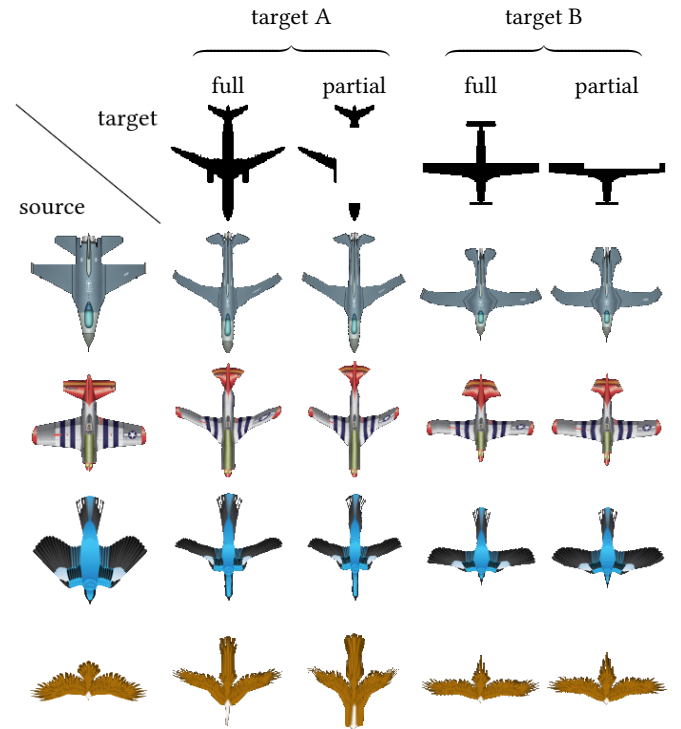


Fig. 2. Examples of partial-shape agnostic deformations (test set). ALIGNNet computes a deformation between source (left column) and full target (A/B) that is nearly identical to the deformation between source and a significantly partial target (A/B). The symmetry of airplane wings is preserved when one wing is missing in target A. Despite the ambiguous length of partial target B, the vertical scale is correctly estimated. ALIGNNet, trained on the airplane class, generalizes well to birds (bottom rows), a completely novel class. Note: RGB textures are applied post-deformation for visualization purposes only (not considered by network).

To handle partial shapes, approaches such as RANSAC [Fischler and Bolles 1981], sample a small number of points to form candidate transformation models, and determine the best one by voting. This approach works well when the two shapes share similar geometries [Aiger et al. 2008], and the transformation model can be expressed with a rather small number of variables, e.g., rigid or affine transformation. However, their search space becomes prohibitively large and even intractable if their geometries significantly differ. Later, we show (Figure 22) a restrictive alignment between shapes using affine transformations. The shapes that we successfully align in our work require higher order deformations, for example FFDs with 128 degrees of freedom.

The use of local descriptors compensates for significant geometry differences [Belongie et al. 2002; Ling and Jacobs 2007; Mori and Malik 2003; Thayananthan et al. 2003; Zheng and Doermann 2006]. Works which use functional maps for correspondence rely on good local descriptors to drive the matching process [Litany et al. 2017]. These descriptors are typically hand-crafted and often tailored to a

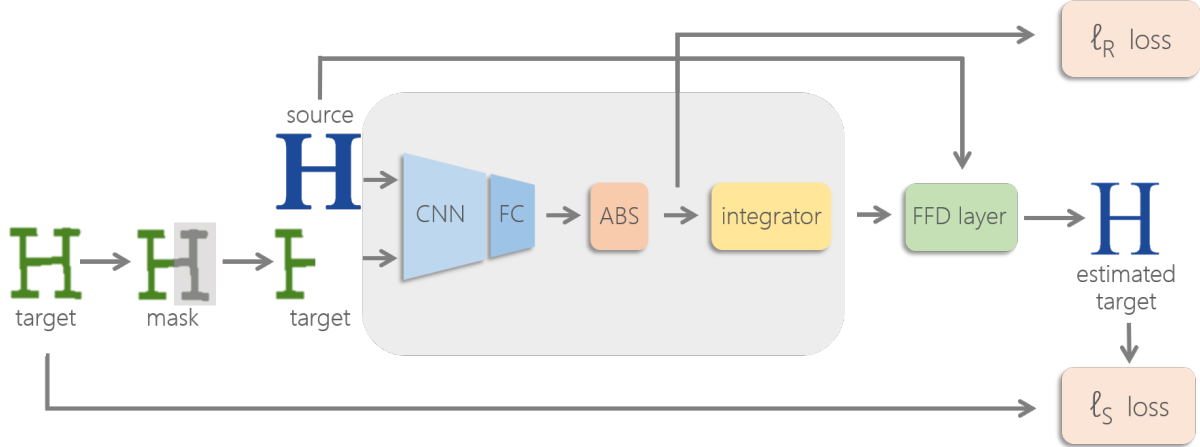


Fig. 3. Illustration of ALIGNet architecture. During training, ALIGNet learns to compute FFD grids without labeled ground-truth FFDs via the proposed unsupervised training scheme. Given input source and target shapes, a random mask is applied to the target shape to form its partial version. A feature extraction CNN and a fully connected (FC) plus absolute value layer are then employed to output the differential of the warp field. The integrator layer, implemented via cumulative sum, results in the warp field. To compute the shape loss ℓ_s , the warp field is applied on the source shape through the FFD warping layer, and the regularization loss ℓ_r is computed on the differential warp field. At test time, after the network weights have been learned, only the sub-partition of ALIGNet that computes the FFD grid deformation is required (bounded inside the gray rectangle).

specific subset of shapes. When the transformation model is a high-order deformation, it is challenging to find good correspondences between the local descriptors, which are often ambiguous.

Recently, many works have taken a deep learning approach to directly compute correspondence or learn an invariant feature descriptor, e.g., [Choy et al. 2016; Simo-Serra et al. 2015; Tian and Wu 2017]. WarpNet [Kanazawa et al. 2016] uses exemplar warps for training a network to compute visual correspondences. Zboncar et al. [2016] train a CNN to accurately match correspondences across stereo image pairs (later improved by [Shaked and Wolf 2016]). Fischer et. al. [2015] proposed using supervised CNNs to solve the optical flow estimation problem. In 3D, Zeng et al. [2017] used 3D-CNNs to learn a noise invariant feature representation. Yumer & Mitra [2016] pioneered the idea of 3D shape deformation using deformation fields. To achieve their goal, they incorporated semantic words in a supervised learning setting (e.g., deforming a car to become more *sporty*). Tewari et al. [2017] estimated facial parameters (such as expression and lighting) from images via an end-to-end autoencoder. Garg et al. [2016] used self-supervision for estimating depth from a single image.

The Spatial Transformer Network (STN) [Jaderberg et al. 2015] showed that incorporating a transformation module into the network enables the task at hand to be transformation invariant (further expanded in [Li et al. 2017]), demonstrating inspiring results on digit classification. ALIGNet can be considered of as a new class of high-order spatial transformers, designed for the task of partial shape non-rigid alignment. In our presented work, ALIGNet learns an FFD, however it can similarly learn other classes of transformations, such as affine, projective or TPS [Bookstein 1989], as used in STN. Note that unlike any of the aforementioned works, we deliberately learn to align a source shape to an incomplete target shape, as though the target were complete.

3 OVERVIEW

ALIGNet is a neural network that aligns a source shape to a target shape via FFD. The FFD controllers are defined on a uniform grid, whose resolution trades off between deformation expressiveness and warping smoothness. Defining the FFD on a uniform grid is a judicious technique for providing an expressive, yet smooth, deformation, with a relatively small number of parameters. The power of ALIGNet lies in its ability to learn to align a source shape to an incomplete target shape as though the target were complete.

Training a network when ground-truth information is unavailable is a major challenge. Our approach employs unsupervised learning, i.e., the true FFD that best aligns the source shape to the target is not utilized during training. The network scheme is illustrated in Figure 3. ALIGNet is trained by drawing two instances from a pool of training data of objects from the same class, deeming one instance as the source shape and the other as the target shape. To mimic missing data, we remove a random part of the target shape, and feed the partial target as input to the network, holding out the full shape for loss computation. The input shapes are then fed forward through a series of neural network layers yielding an FFD, which when applied on the source shape yields a deformed source, called the estimated target. The training loss measures the difference between the estimated target and the complete target. Consequently, ALIGNet is *partial shape agnostic*, that is, it learns to estimate the deformation that aligns the source shape to the partial target as if it were the complete target.

Without any restrictions on the FFD, ALIGNet can conjure up deformations which do not preserve internal structure. To this end, we introduce a total variation penalty that is key to producing smooth deformations. Rather than directly computing the *actual displacement* values, we compute *relative displacements*, where each displacement is relative to its preceding displacement, such that

the cumulative summed result (in each axis) yields the actual grid displacement field. Since these relative displacements are essentially displacement gradients, we utilize them to employ anisotropic total variation (TV) on the deviation from the identity warp field, which encourages uniformly spaced piecewise smooth deformation fields. To further encourage smoothness, we maintain axial monotonicity by enforcing positive relative grid displacements which ensure consecutively increasing values in each axis of the displacement grid. We present and evaluate ALIGNet on 2D shapes, and demonstrate its extension to 3D in section 5.4.

4 METHOD

The input to our system is made up of pairs of source and target shapes, where a target shape may be partial at various locations and to varying extents. The baseline system consists of a neural network component f that computes an FFD in the form of a grid-based warp field W_c . The input source shape S and the potentially partial target T^p are stacked as a two-channel image and passed to f to obtain the low resolution FFD warp field: $f(S, T^p) = W_c$. The architecture of f is given by a series of max pooling, convolutions and rectified linear activation units (repeated four times), followed by two fully-connected layers. Similar to [Jaderberg et al. 2015], we train the network from scratch by setting the convolutional layer weights randomly, and initializing the last FC to yield the identity displacement field (weights set to zero and biases to the identity displacement field). This is followed by the differentiable FFD sampling layer, which warps the source to the target by upsampling the low resolution FFD.

The network is trained in an unsupervised manner, such that at no point during training is it shown the ground-truth warp field that correctly aligns the source to the target shape. Instead, the pairs of shapes given as input during training are in fact triplets, where the target is passed twice - once in its complete form and once with missing parts. This scheme facilitates training by bestowing a self-supervised shape similarity loss function (ℓ_s): comparing the warped source to the full target (see Figure 3), aimed at teaching the network to become oblivious to possible missing data.

In addition to the shape similarity loss function, we add a regularization loss (ℓ_r) which encourages the network to produce a warp field that is varying uniformly vis-à-vis the identity warp, limiting the likelihood of fold-overs. Our loss function thus amounts to: $loss = \ell_s + \lambda \ell_r$, where λ is a user defined parameter that trades off between shape alignment and smoothness of the warp field.

4.1 FFD Representation

We constrain the space of possible warp fields by incorporating regularization that encourages piecewise smooth deformation fields and simultaneously enforces axial monotonicity (illustrated in Figure 5). We facilitate these warp field constraints by representing the FFD as a *differential* displacement grid, where each value is relative to the preceding value in the grid. Instead of directly computing the absolute FFD values after the FC layer, we compute the differential FFD values, which when cumulatively summed result in an absolute FFD grid. The differential displacement grids encourage shift-invariance, since the displacement at each grid cell is relative to its neighborhood.

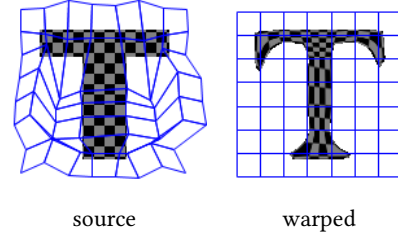


Fig. 4. 2D FFD grid deformation. The uniform 8x8 grid in the warped domain (right) shown in blue, applied in a backwards manner: each location in the warped domain grid corresponds to a look-up location in the source (left).

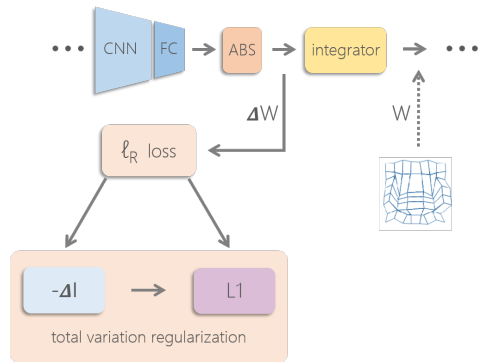


Fig. 5. Regularization component commissioned for training ALIGNet to compute plausible FFD grids. The network weights predict a differential grid, passed through an absolute value operator to enforce axial monotonicity. Followed by ℓ_1 regularization on $\Delta W - \Delta I$ (equivalent to anisotropic total variation regularization on $W - I$). Lastly, the differential cumsum layer (Integrator) restores the absolute displacement grid.

To illustrate differential displacement fields, consider a 1D absolute sequence a of length n , and the corresponding differential sequence Δa as

$$a = \{a_k\}_{k=1}^n = (a_1, a_2, a_3, \dots, a_n) \quad (1a)$$

$$\Delta a = \{a_k - a_{k-1}\}_{k=1}^n = (\Delta a_1, \Delta a_2, \Delta a_3, \dots, \Delta a_n) \\ = (a_1 - a_0, a_2 - a_1, a_3 - a_2, \dots, a_n - a_{n-1}), \quad (1b)$$

where a_0 is a scalar offset (here $a_0 = 0$) that can be learned during training. Given the differential 1D Δa , the absolute sequence can be exactly recovered using the cumulative sum operator

$$a = \text{cumsum}(\Delta a, a_0) = \left\{a_0 + \sum_{i=1}^k \Delta a_i\right\}_{k=1}^n. \quad (2)$$

The proposed cumsum layer is differentiable and can be added into a network for training. It is apparent in the 1D example that the derivative is given by

$$\partial \Delta a = \left\{\sum_{i=k}^n \partial a_i\right\}_{k=1}^n. \quad (3)$$

The deformation field in ALIGNet is a 2D grid with vertical and horizontal displacement components, where the cumsum operates along each dimension, respectively. The learned ALIGNet weights map the input shapes to the differential displacement field ΔW_c , subsequently passing through the absolute and cumsum-layer, resulting in the final displacement field $W_c = \text{cumsum}(\Delta W_c, W_0)$ (where W_0 is a learned scalar).

Axial Monotonicity. Observe that for any strictly positive differential 1D sequence ($\Delta a_k \geq 0$ for all k), the recovered absolute 1D sequence a is monotonic

$$a = \left\{ a_k \right\}_{k=1}^n \quad \text{s.t. } a_k \leq a_{k+1} \quad (4)$$

In ALIGNet, we enforce the differential sequence at the end of the network to be positive. In the 2D case, enforcing strictly positive relative displacement values $\Delta W_c \geq 0$, we ensure axial monotonicity in the displacement fields. Axial monotonicity implies that each axis increases monotonically independently of the opposing axis.

FFD Layer. The displacement map used to express the FFD is a low resolution 2D displacement grid, defining the inverse warp field from target to source (see Figure 4). To obtain the full resolution target image, pixels in the target image are copied from their corresponding source image locations as indicated by a bilinear interpolation upsampling of the low resolution warp field. This is accomplished by a 2-step bilinear sampling operation. First, use the bilinear sampler \otimes to upsample the lower resolution grid W_c to the full size of the source image ($m \times n$) by $W = W_c \otimes G^{m \times n}$, where $G^{m \times n}$ is a regular grid of coordinates for every pixel in the full resolution $m \times n$. The second sampling applies the upsampled warp field on the source shape $\hat{T} = S \otimes W$, resulting in an estimate of the target shape. For brevity, we represent the two-step sampling as

$$\hat{T} = S \otimes W_c \leftarrow S \otimes (W_c \otimes G^{m \times n}). \quad (5)$$

4.2 Loss Functions

Estimating FFDs without direct supervision is ill-posed, since the large degree of freedom (DoF) in the FFD results in wildly different deformations - all with very similar cost. Specifically, ALIGNet operates solely on binary silhouettes, since knowing the true corresponding RGB textures between source and target shapes requires a form of ground-truth annotation. Binary silhouettes are problematic since any FFD that deforms source foreground pixels to target foreground pixels, even if parts are completely rearranged, results in the same shape similarity loss. Absent regularization, ALIGNet is entitled to falsely conjecture about the possible deformation field.

Our overall loss function is composed of two components. The first is the shape alignment loss, encouraging a faithful deformation from source to target. The second, which measures anisotropic total variation with regards to deviation from the identity warp, serves as a strong regularization component that helps produce smoother warp fields.

4.2.1 Shape Alignment Loss. The self-supervised training loss evaluates the difference between the complete target T and the source that has been aligned by the FFD (*i.e.*, estimated target \hat{T}) to train ALIGNet. For every example n (S^n, T^n) in the training set \mathcal{N} ,

we train the network by minimizing the loss given by

$$f = \arg \min_f \sum_{n \in \mathcal{N}} \|S^n \otimes f(S^n, T^{p^n}) - T^n\| = \sum_{n \in \mathcal{N}} \|S^n \otimes W_c - T^n\|, \quad (6)$$

where $\|\cdot\|$ can be any error measure. We use the ℓ_2 -norm, which is given by

$$\ell_s(T, \hat{T}) = \sum_{i \in \mathbb{V}(\hat{T}, T)} \frac{1}{2}(T_i - \hat{T}_i)^2, \quad (7)$$

for every pixel i in the target and estimated target.

The proposed approach enables training without ground-truth FFDs while simultaneously learning to be partial-shape agnostic. At test time, given a source shape S and a target shape with different parts missing $T^{p^1}, T^{p^2}, \dots, T^{p^n} \in T$ (from test set), ALIGNet demonstrates partiality-agnostic behavior by computing very similar FFDs for different partialities of the same underlying target (see Figure 13). We attribute this generalization to the unsupervised nature of the training process.

4.2.2 Anisotropic Total Variation Identity Regularization. We facilitate minimal distortion deformation fields by imposing an additional penalty in the form of TV regularization. Observe that the differential sequence as defined in Equation 1b, is actually the discrete gradient of the absolute sequence in Equation 1a. Similarly for the 2D counterpart, the differential grid ΔW is made up of two channels, $\Delta W_x, \Delta W_y$, which are the horizontal and vertical derivatives of W respectively. Recall that the anisotropic total variation regularization for a 2D matrix is given by the ℓ_1 -norm of the sum of the horizontal and vertical gradients

$$\ell_{TV}(W) = \|\Delta W_x\|_1 + \|\Delta W_y\|_1. \quad (8)$$

TV regularization encourages deformations that are piecewise smooth, favoring smoothness but simultaneously allowing for large discontinuities due to the ℓ_1 -norm. Piecewise smoothness is the essence of a favorable deformation field: large discontinuities at the shape boundaries with a smooth shape interior.

Yet, the displacement field W that would lead to the lowest cost in the standard TV regularization in Equation 8 would be simply a zero valued differential displacement field, which is an undesirable result. Instead, we encourage a non-zero-valued uniform spacing by subtracting the differential identity warp field from the differential warp, favoring a uniformly spaced grid over the size of the image.

For a 1D analogy, consider an identity sequence I of length n normalized to the interval $[-1, 1]$, which is uniformly spaced by a scalar $\delta_k = \frac{2}{n-1}$. Then we can write I and the corresponding differential ΔI as

$$I = \left\{ -1 + (k-1) \cdot \delta_k \right\}_{k=1}^n = (-1, -1 + \delta_k, -1 + 2\delta_k, \dots, 1) \quad (9a)$$

$$\Delta I = \left\{ \delta_k \right\}_{k=1}^n, \quad (9b)$$

where the differential identity sequence ΔI contains a single unique value: the uniform spacing constant δ_k . In 2D, it follows that the proposed anisotropic TV identity regularization becomes

$$\ell_r = \ell_{TV}(W - I) = \|\Delta W_x - \Delta I_x\|_1 + \|\Delta W_y - \Delta I_y\|_1. \quad (10)$$

Architecture		Parameters	
conv1	$5 \times 5 \times 20$	n	8
conv2	$5 \times 5 \times 20$	m	8
conv3	$2 \times 2 \times 20$	λ	$1e - 5$
conv4	$4 \times 4 \times 20$	solver	ADAM
fc1	20	LR	$1e - 3$
fc2	$2 \cdot m \cdot n$		

Table 1. ALIGNet architecture and parameters used for all results (except where otherwise specified), where m and n represent the resolution of the grid.

The overall contribution of the regularization term is controlled by a weighting factor λ .

5 RESULTS AND EVALUATION

In this section we examine and test ALIGNet through various qualitative and quantitative evaluations (code and data are available at <https://github.com/ranahanocka/ALIGNet>). All experiments are performed on the reserved *test set data*, meaning that these shapes were never trained on. All networks are trained on strictly binary silhouettes, but we overlay a checkerboard texture on the source shape to clearly visualize the smoothness of the estimated mappings and display the texture transfer abilities facilitated by our system. Note that the missing components of the target are illustrated in light pink (for visualization purposes only), but the actual network input is binary. For all results and classes, we use the same parameters and architecture described in Table 1, unless stated otherwise (e.g., in the ablation study).

5.1 Training Data

In our experiments, we train ALIGNet on a class of shapes where pairs of source and target instances are randomly drawn from the pre-defined training set. Specifically, we have experimented with sets containing renders of lower and upper case letters for 330 fonts (resulting in 56 classes), as well as 2D projections of 3D objects from ShapeNet [2015] and COSEG [Wang et al. 2012].

Train and Test Sets. For each class dataset, we reserve 30 models for testing and use the rest for training. For example, a class with a set of 330 shapes yields $\sim 90k$ distinct training pairs and 870 test pairs. We augment the number of training set examples by generating an arbitrarily large amount of partial data, and by applying small vertical and horizontal scaling on-the-fly during training. We generate rectangular partial data masks by setting a random foreground pixel as the center, with width and height sampled from a uniform distribution.

During testing, we evaluate performance on rectangular masks and verify generalization on non-rectangular partial data masks created from the MPEG-7 [Latecki and Lakamper 2000] dataset.

5.2 Ablation Study

We analyze the qualitative and quantitative effects of grid regularization by training ALIGNet in three different settings: without any regularization (none), total variation regularization (TV) and total

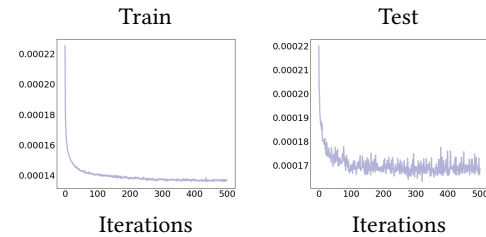


Fig. 6. Train (left) and test (right) error convergence plots for the *vase* class.

variation regularization with axial monotonicity (TV & M). Regularization controls the trade-off between: fidelity, in our case the silhouette alignment accuracy, and the prior, which is the smoothness of the warp field. We quantitatively measure accuracy via IOU between the source and true underlying target, and measure smoothness by the difference between the warp field gradient and the identity field gradient (TV loss in Equation 10).

The fidelity term in ALIGNet (Equation 6) without additional regularization is a greedy criteria, aspiring to improve the alignment accuracy (synonymous to IOU) at any cost. Without any regularization, advanced training iterations yield increasingly unsmooth warp fields. This continued training results in a deceitful improvement in alignment accuracy, since the resulting deformation is inconsistent with plausible FFDs (visuals in Figure 8). Importantly, training with TV regularization preserves smooth fields for increasing training iterations, stipulating faithful improvements in alignment accuracy (plots in Figure 9). Naturally, incorporating an additional regularization term leads to slightly inferior IOU accuracy, but gains significantly smoother, and therefore more conceivable, warp fields.

Furthermore, we explore the effects of varying grid resolutions on deformation smoothness, expressivity and high-frequency oscillations of the shape boundary and internal structure (Figure 10). A grid of very low resolution (e.g., 2×2 or 4×4) produces an inherently low-frequency deformation. Yet, the alignments in these resolutions are noticeably inadequate for the disparate geometries between the airplanes. Conversely, a grid of very high resolution (e.g., 23×23) produces an expressive deformation, which tends to contain redundant oscillations. Note in some cases it may be possible to achieve finer results using a higher grid resolution, this would necessitate more training data, deeper networks, and longer training time. For this reason, we opt for a moderate grid resolution (e.g., 8×8), to produce smooth and expressive deformations.

Additionally, we investigated using an alternative loss function (results in Figure 7), namely isotropic total variation. Recall Equation 8 which defined anisotropic TV, isotropic TV is given by

$$\ell_{TV}(W) = \|\sqrt{\Delta W_x^2 + \Delta W_y^2}\|_1, \quad (11)$$

where the square and square-root operations are applied element-wise.

5.3 ALIGNet Generalization

In this section we demonstrate the generalization capabilities of ALIGNet. We show test results on novel classes with similar characteristics, demonstrating ALIGNet does not over-fit or memorize

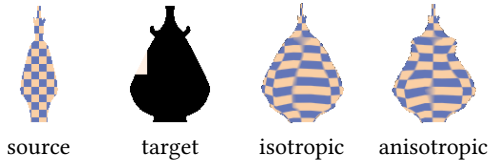


Fig. 7. ALIGNet is modular, with the ability to employ alternative forms of regularization depending on the application. Applying isotropic vs. anisotropic TV regularization can lead to slight differences in the outcome.

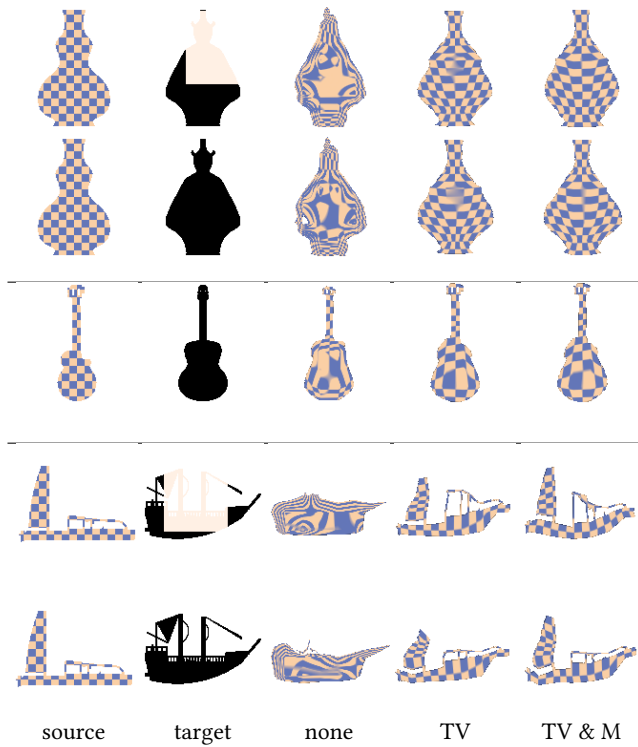


Fig. 8. Ablation study visual examples for increasing levels of FFD regularization: no regularization, TV regularization and TV regularization with axial monotonicity. Without regularization, ALIGNet is not partial agnostic: the deformation is disparate for the full and partial version of the same target.

the training data. We deform a novel class source to a target from the class trained on in Figure 11. For example, consider the top section of Figure 11, where ALIGNet trained on vases is used to align a pear and a pumpkin source shapes (novel yet geometrically similar classes) to vases from the test set, resulting in *pear-esque* and *pumpkin-esque* vases. We demonstrate further generalization abilities in Figure 12, where we utilize a network trained on a certain class to perform alignments from source to target such that *both* belong to a novel class. Figure 13 features similarly predicted ALIGNet alignments for the same source and underlying target, with differing missing element locations. This missing part location indifference simultaneously demonstrates missing part generalization and partial agnosticism of ALIGNet. Similarly, in Figure 14, we

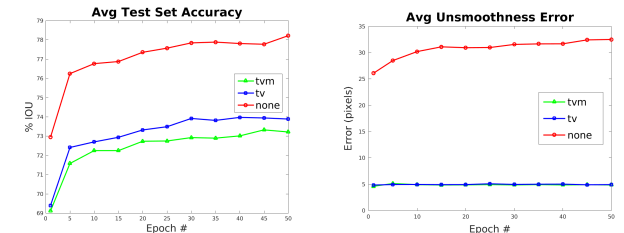


Fig. 9. Quantitative ablation study for no regularization (none: red), total variation regularization (tv: blue) and total variation regularization plus axial monotonicity (tvm: green). Left: increasing gains in accuracy do not necessarily correspond to plausible warp fields (visuals in Figure 8). Right: observe that without regularization the unsmoothness error metric (Equation 10) increases as training advances, however the smoothness remains constant with regularization present.

present a *stress test* on the same source and underlying target by computing alignments for an increasing amount of missing data in the target. Observe that the estimated mappings are initially predicted consistently, and even when significant portions of the data are missing, the estimated mappings remain plausible.

5.4 Applications in 3D

Throughout the paper we have shown alignment results obtained by applying ALIGNet on shapes within the 2D domain, and demonstrated the integrity of the estimated warps and their readiness to support alternative post-process 2D applications. In this section, we shift our focus to the 3D domain, and present additional applications following a simple extension of ALIGNet to 3D. We train on volumetric data (of resolution 32x32x32) and replace the convolution, pooling, integrator and FFD layer modules with their 3D counterparts. We learn to regress an FFD grid of resolution 7x7x7 (1029 DoF), which is applied directly on the source mesh vertices. Note that neither the grid nor voxelization resolution affect the quality of the output mesh, since the deformation is applied on the input high-resolution mesh. See Figure 15 for a visualization of our 3D grid.

Volumetric CNNs typically operate on voxelized shape representations where not only is the surface of the shape marked as occupied, but also the inner volume. Generating a voxelized representation of surface-based shapes represented, e.g., as meshes, is straight-forward. The same, however, cannot be said for shapes represented, e.g., as point clouds, which sparsely sample the surface of an object. To this end, we train ALIGNet on (hollow) volumetric surfaces automatically generated from 3D meshes. During training, we draw pairs of source and target shapes from the pool of voxelized surfaces, and remove random portions from the target surface. As in 2D, we train ALIGNet by comparing the overlap between the warped source surface and the expected (complete) target surface. While the 3D grid is estimated for the voxelized surface, we can simply apply it on the original mesh. Below we show applications of 3D warping on point-cloud registration and segmentation transfer.

Point Cloud Registration. In many applications ranging from VR and AR to scene understanding, it is desirable to align a mesh



Fig. 10. Grid resolution expressiveness. We experiment with increasing grid resolutions to explore the change in warping flexibility. Results were obtained using ALIGNet under the exact same conditions, apart from grid size. Observe that a smaller grid resolution facilitates a smooth but not expressive enough deformation, while a higher resolution yields a deformation that is more expressive but contains redundant deformations.

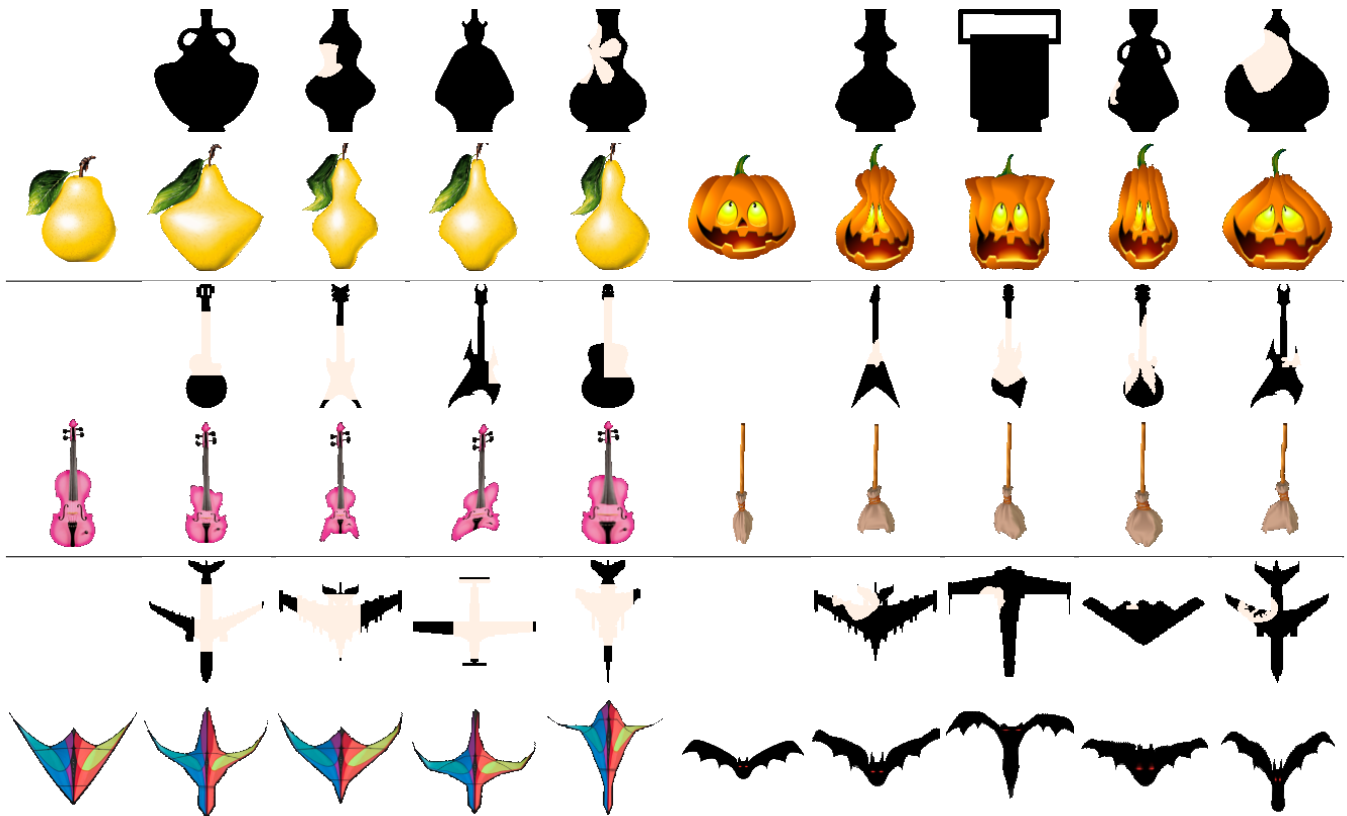


Fig. 11. Qualitative results of applying ALIGNet to untrained classes. We utilize ALIGNet trained on three different classes to deform source shapes from novel classes (untrained) that share geometric commonalities with one of the trained classes. In these examples, we deform a *pear* and a *pumpkin* into *vases* (top), a *violin* and a *broom* into *guitars* (middle) and a *kite* and a *bat* into *airplanes* (bottom).

(containing semantic information) to a partial point cloud obtained by a scanning device. Figure 16 features several examples of alignments performed between 3D meshes and point clouds using our method (quantitative results in Table 2). Recall that our 3D network processes pairs of voxelized surfaces as input, such that the source is complete, and the target is generated from a complete surface by removing parts at random. At test time, however, we are given a target shape represented as a point cloud, requiring conversion into our network format. To this end, we simply discretize the continuous coordinates of the point cloud and form a sparse surface occupancy grid. Despite not having trained on such sparsely

sampled surfaces, ALIGNet generalizes well and is able to produce plausible deformations.

Segmentation Transfer. Semantically segmenting a shape into its constituent parts is an important first step for a wide range of applications in shape analysis and synthesis. A popular approach to solve this task is the transfer of an existing high-quality segmentation from one shape to another. Naturally, some form of correspondence between the two shapes must be given or computed in order to support the transference.

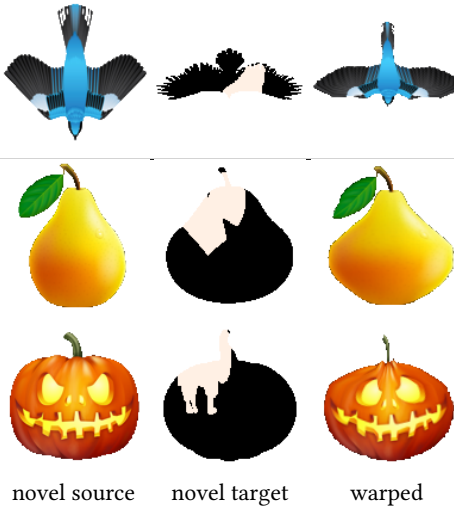


Fig. 12. Qualitative results of applying ALIGNet to untrained classes. Both source and target shapes belong to novel classes that were not trained on, yet they share geometric commonalities with the trained class. The top row features a *bird-to-bird* deformation, performed using ALIGNet trained on *airplanes*, while in the bottom two rows, *pear-to-pear* and *pumpkin-to-pumpkin* deformations are carried out using a *vase*-trained network.

samples	500	3000
IOU	53	57

Table 2. Quantitative results for 3D point cloud registration on the *airplane* class. We compute the average IOU between deformed source and full target given target in point cloud form for both 500 and 3000 point samples. Note that the IOU is computed on the full voxelized representation of the shapes generated from their mesh forms, where the applied warp field is computed using the point cloud representation of the target.

To further demonstrate the integrity of ALIGNet warps, we show results on segmentation transfer in 3D. Using the same trained model that was used in the previous application (Figure 16), we estimate the deformation between a segmented (source) shape and an unsegmented (target) shape. Given the underlying correspondence determined by the alignment, we transfer the segmentation labels from the source shape faces to their corresponding faces on the target shape, and perform a simple graph cut optimization to obtain a complete and smooth result (see Figure 17).

5.5 Robustness

Symmetry. Bilateral symmetry is characteristic of many man-made as well as natural shapes. Accordingly, most of our datasets are composed either entirely, or almost entirely, of bilaterally symmetric shapes. We have shown that our system is able to recover such symmetries even when a target is missing portions in a pattern that impairs the original symmetry of the shape. However, symmetry is a strong cue that often assists in tasks of reconstruction, and it is possible that ALIGNet is more easily trained on a dataset that is inherently symmetric.

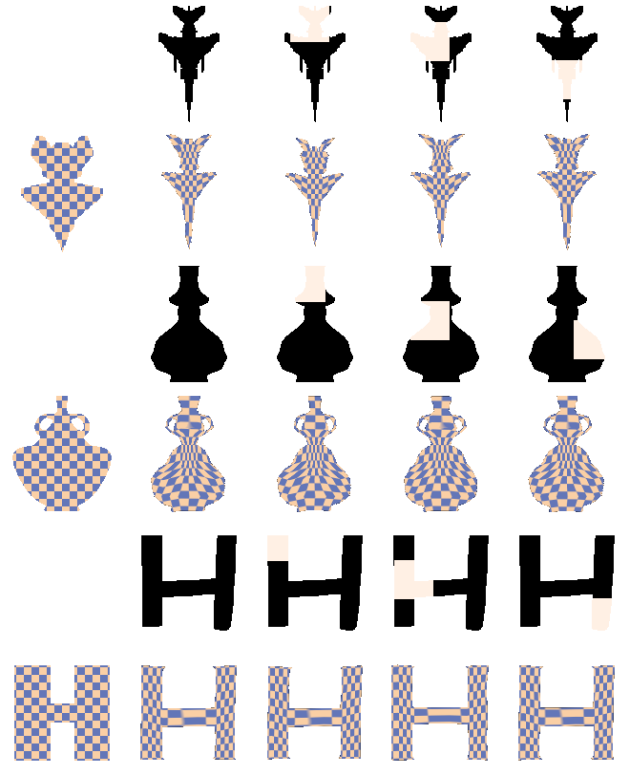


Fig. 13. Qualitative demonstration of network generalization and partial-agnostic behavior. Displayed are examples from the test set for three different classes (top: *airplane*, middle: *vase*, bottom: *uppercase H*). The warp computed by ALIGNet on a particular source and different partialities of the same target results in a visually consistent deformed shape.

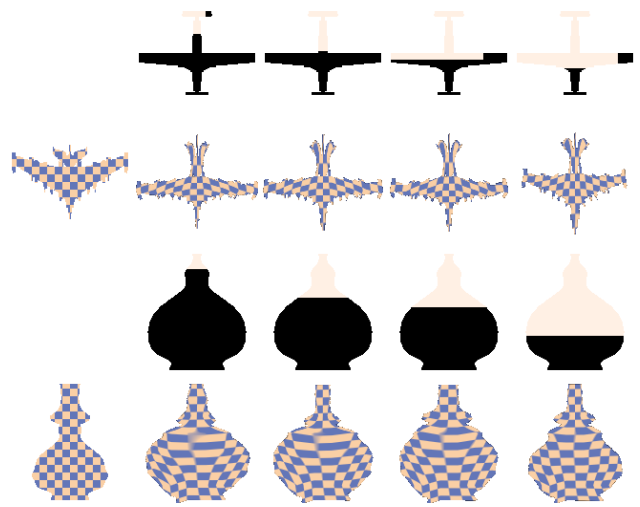


Fig. 14. Qualitative stress test for FFD computation under increasing percentage of missing shape data.

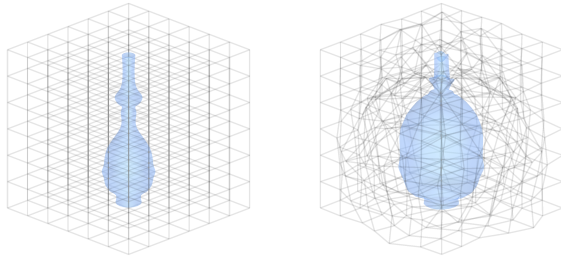


Fig. 15. 3D deformation grid. The source shape is placed within the uniform $7 \times 7 \times 7$ grid (left). A deformation on the grid induces the shape to warp as shown on the right.

We are therefore particularly interested in examining the performance of ALIGNet on datasets that are asymmetric in nature. Examples for alignments performed on rendered asymmetric letters ("C" and "L") are presented in Figure 18. We observe the satisfactory recovery of the structure of the shapes, suggesting that our approach does not require symmetry as a leading prior to learn to align.

Orientation. Our baseline experimental setting assumes that input datasets are consistently pre-oriented, an assumption that holds for many readily available shape datasets. Where this assumption does not hold, consistent orientation methods can be employed (e.g. hierarchical alignment [Chang et al. 2015]). Even so, we investigate the ability of our system to handle orientation errors.

We augment our dataset by introducing rotations uniformly sampled from the range $[-30^\circ, 30^\circ]$, and train ALIGNet as previously described. Figure 19 shows the qualitative alignment results of our augmented network trained on shapes with arbitrary rotations.

Multi Class. A core strength of ALIGNet lies in the higher level understanding of a particular shape category, enabling it to preserve geometric features that are typical to the class of objects at hand. However, we investigate the robustness of ALIGNet to handle multiple classes simultaneously. By sampling three different classes during training, using the same architecture, we observe that ALIGNet can jointly handle several classes simultaneously (see Figure 20).

To further assess the scalability of ALIGNet, we train a single network on an increasing number of classes. We begin with our baseline of single-class training, and add a new class at each step, up to a total of six classes. In Figure 21 we deform a source shape to two different targets from the airplane class, and track the results as the number of trained classes increases. We note the apparent degradation exhibited in the top row, versus the very slight degradation in the bottom row. These results align with our expectations for the general robustness and scalability of the network, accompanied by a little degradation that is a natural outcome of the strain placed on the network as we load more and more classes. To mitigate the effects of degradation, one can consider deepening and widening the network to allow for a larger capacity of shape priors.

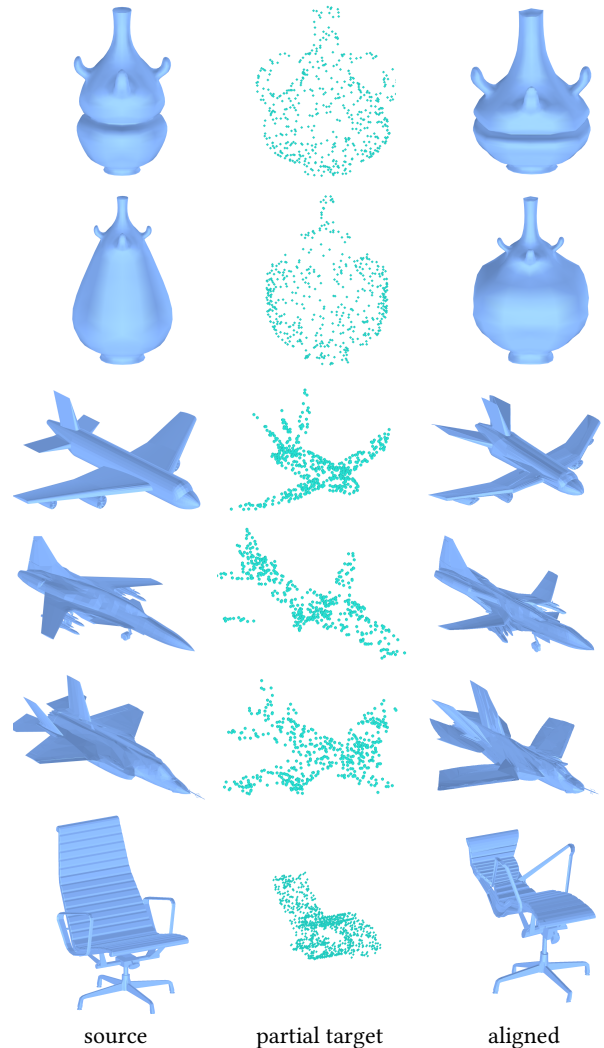


Fig. 16. Aligning a high quality 3D mesh to a point cloud. ALIGNet estimates the $7 \times 7 \times 7$ grid deformation between a 3D source mesh (represented as a complete voxelized surface) and a point cloud (sparse voxelized surface), which we apply on the vertices of the source mesh to obtain the aligned version (last column). ALIGNet, trained on complete surfaces with segments removed at random, generalizes to sparse surfaces at test time.

5.6 Comparisons

In this section we compare the results of applying ALIGNet, versus existing approaches, on the 870 reserved test set pairs for each class (as described in Section 5.1). The quantitative results are summarized in Table 3, with visual examples shown in Figure 22.

Since existing approaches usually operate on point-sets, we compute the deformations on the contour of the shapes. For comparable results, we apply the contour deformation on the entire image. The high order deformation computed using CPD [Myronenko and Song 2010] contains two regularization parameters: first to control deformation field smoothness, and second to control the distortion allowed on the source shape. Setting the CPD deformation field

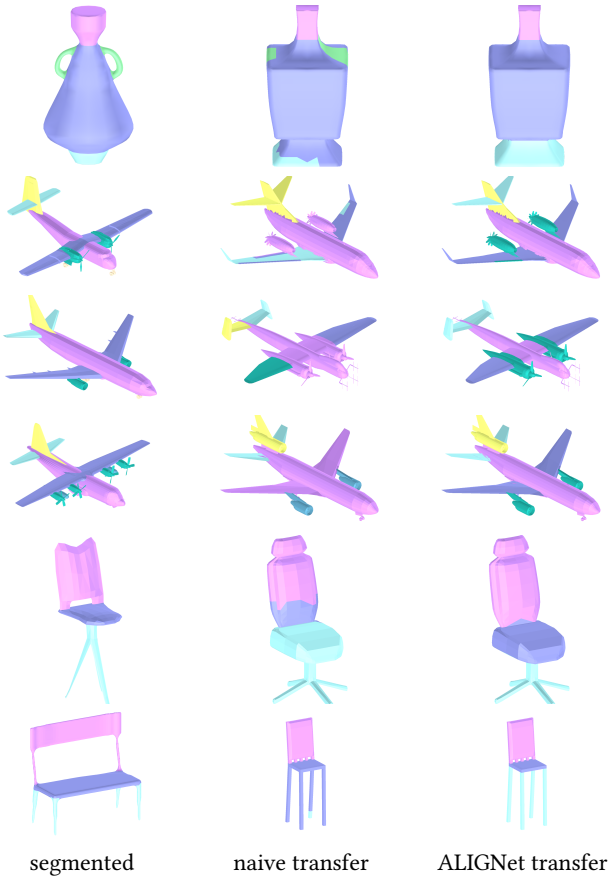


Fig. 17. ALIGNet results on 3D segmentation transfer (test set). The labels in the source shape (left) transferred to the target shapes using the correspondence generated with ALIGNet (right). The estimated alignment is used in combination with a simple graph cut optimization as a post process. In the middle column, we compare to a baseline transfer, where the identity warp is used to guide the correspondence.

smoothness weight too high restricts the expressiveness allowed in the warp field (similar phenomenon as in ALIGNet). However, the parameter which controls the source shape distortion is trickier; a large weight restricts the source shape from conforming to the partial components while also restricting the source shape to conform to the target. We also show results of the shape context descriptor (SC), matching and alignment of [Belongie et al. 2002]. In addition to the global and local structure preserving point set registration (PRGLS) of [Ma et al. 2016].

To demonstrate the restrictiveness of lower order deformations, we present two different affine transformation results. The first, a RANSAC-based approach, samples three points on the source and target to compute an affine transformation, and selects the best transformation based on source and target voting. Since the aforementioned approaches do not estimate alignment parameters cognizant of the attributes specific to a particular class, estimating simple parameters such as scale becomes difficult (see last row of



Fig. 18. Examples of alignment of asymmetrical shapes.

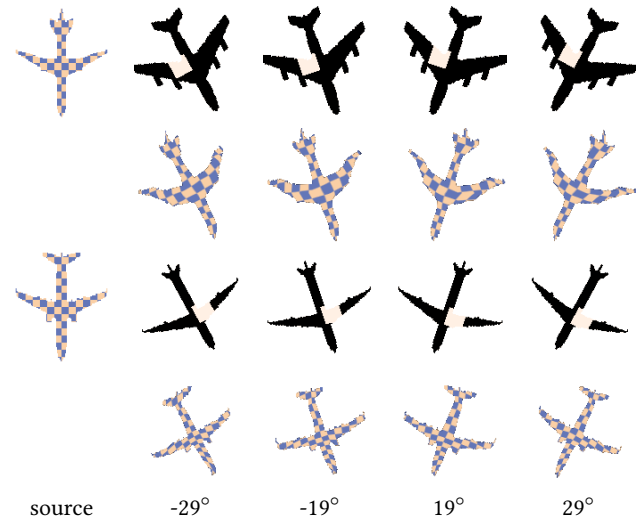


Fig. 19. Robustness to orientation deviations by adding data augmentation: training on offsets within the range $[-30^\circ, 30^\circ]$. Test results shown for orientation offsets of -29° , -19° , 19° and 29° for the same source and target pairs.

Figure 22). To this end, we create an additional data-driven learning-based approach against which to compare. Using the implementation of Spatial Transformer Networks (STN) [2015] (available in the form of an affine transformation), we train the STN network *vis-a-vis* ALIGNet. We train STN using the same architecture, data and learning parameters as ALIGNet, but without the regularization components (superfluous for low DoF deformations).

Observe that both learning approaches, STN and ALIGNet, are better suited to preserve features characteristic to the class of objects being warped (Figure 22). However, the limiting DoF in STN is often

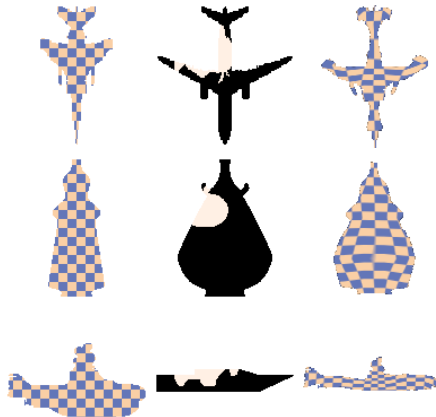


Fig. 20. Results of a single ALIGNNet network trained on three classes.

vase	IOU	airplane	IOU	vessel	IOU
ALIGNet	81.3	ALIGNet	69.0	ALIGNet	60.2
CPD	62.8	CPD	44.2	CPD	40.7
CPD affine	58.9	CPD affine	37.2	CPD affine	37.9
PRGLS	47.8	PRGLS	18.5	PRGLS	25.7
SC	48.1	SC	36.8	SC	39.8
STN	74.1	STN	57.2	STN	59.6

Table 3. Quantitative results of average IOU on the entire test set of the *vase*, *airplane* and *vessel* classes. All approaches use a fixed set of parameters for all classes. We compute ALIGNet results using TV & M regularization.

over-restrictive, which prevents the scale from being accurately recovered (see rows 2 & 3 Figure 22).

Full Shapes. While a core asset of ALIGNet is its ability to handle partial shapes, we are interested in the performance of our system in a simpler setting of complete shapes, and extend our evaluation accordingly. The quantitative results are summarized in Table 4, with visual examples shown in Figure 23.

ALIGNet uses the learned prior to compute full-shape warps that maintain shape semantics post-alignment (see Figure 23). Observe that non-data-driven approaches often struggle to preserve shape features, for instance the symmetry of vase handles in rows (a) and (b), or the airplane tail in (e). Lastly, many of the non-data-driven approaches use a regularization term to encourage smooth contour-to-contour deformations which may result in a less accurate alignment (see row (d) and quantitatively in Table 4).

5.7 Limitations

We note that a grid-based deformation limits the space of transformations that the shape can undergo for alignment. A finer resolution increases the degrees of freedom and becomes more susceptible to implausible deformations, which we have shown can be mitigated with an appropriate regularization mechanism. However, as can be seen in Figure 10, when the degree of deformation is too large compared to the network size, even our regularization term will not

vase	IOU	airplane	IOU	vessel	IOU
ALIGNet	81.3	ALIGNet	70.3	ALIGNet	63.7
CPD	75.2	CPD	57.6	CPD	55.9
CPD affine	69.9	CPD affine	49.3	CPD affine	48.0
PRGLS	55.7	PRGLS	26.9	PRGLS	33.4
SC	70.3	SC	59.1	SC	50.2
STN	74.1	STN	57.3	STN	61.5

Table 4. Quantitative results on complete (not partial) shapes. Average IOU on the entire test set of the *vase*, *airplane* and *vessel* classes. All approaches use a fixed set of parameters for all classes. We compute ALIGNet results using TV & M regularization.

suffice. While the proposed approach produces complex deformations even with regularization, we recognize that such a step in itself results in a confinement of the deformation expressiveness. The proposed approach cannot handle large differences in topologies. Furthermore, our grid-based deformation would not be an appropriate method of transformation for shapes with articulations. We have shown how to incorporate an unsupervised global orientation estimation into ALIGNet in Figure 19. However, these results suggest that a more comprehensive solution may be necessary to achieve higher orientation and shape alignment quality.

6 CONCLUSION

Aligning one shape to another with a high order deformation is a fundamentally ill-posed problem, but when missing parts are thrown into the mix, the ambiguity only deepens. Classic alignment techniques are often at a loss under such circumstances, as the missing information can be highly misleading. To alleviate this, we take advantage of large collections of shapes, and train a system to align pairs of source and potentially partial target shapes. The system learns the space of plausible deformations associated with the dataset, and effectively becomes agnostic to missing parts, without memorization or over-fitting.

A notable advantage of our approach lies in its regressive nature. Instead of synthesizing completely new shapes from scratch, we learn to align one shape to another, resulting in a tool that enables us to deform a high quality source shape to a low quality target, thereby forming novel instances. By taking this route, we simplify the learning process, requiring a smaller network that is less sensitive and able to converge faster.

Our technique introduces a key contribution in the form of a regularization mechanism that promotes smoothness. We have shown (Figure 8) that allowing the system to run wild with its free form deformation computations is not only detrimental to structure preservation, which is crucial for post processing (e.g., texture & segmentation transfer and preserving 3D geometry), but also hinders partial agnosticism. Our regularization relies on a differential grid deformation that naturally supports a total variation penalty encouraging piecewise smooth warps.

The benefits associated with data-driven paradigms are central to the performance of our system. The information contained in the training data assists the network to learn a shape prior that helps preserve the characteristic features of the input set of shapes.

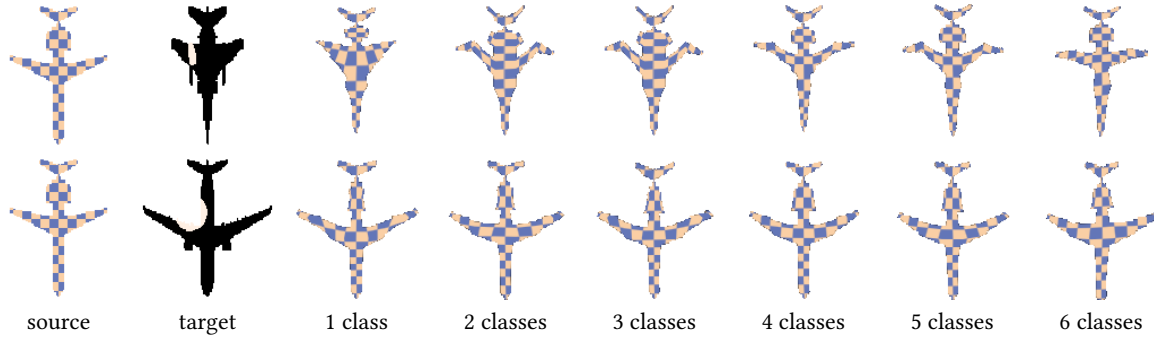


Fig. 21. Robustness of a single ALIGNet network to handle a large number of classes. Given the same network architecture, we incrementally increase the number of trained classes from one class to six (*airplane, vase, vessel, guitar, uppercase L and bottle*). Observe that while there is little to no degradation for some examples (bottom row), there is a more pronounced performance degradation in others (top row).

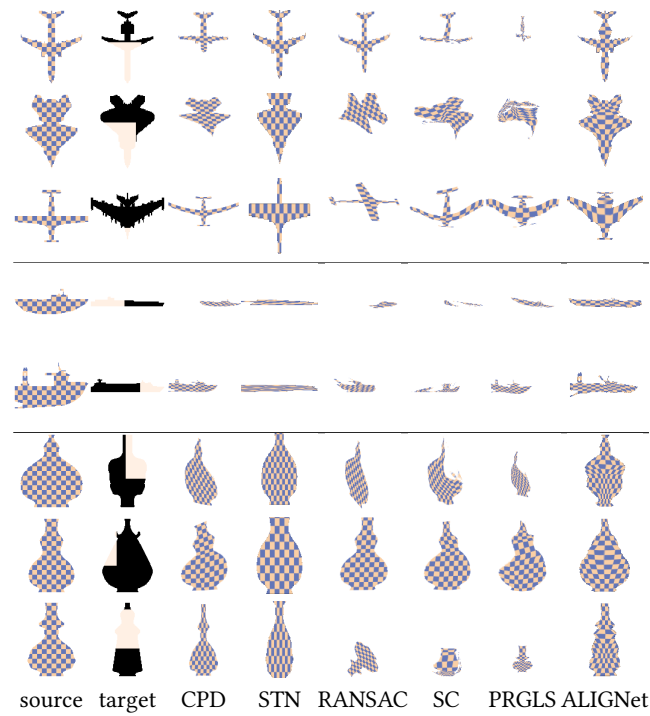


Fig. 22. Visual examples of test set results for: CPD [Myronenko and Song 2010], STN [Jaderberg et al. 2015] (in ALIGNet framework), affine RANSAC, SC [Belongie et al. 2002], PRGLS [Ma et al. 2016] and our method. The same set of parameters is used across all examples for ALIGNet and existing approaches. Observe that ALIGNet is able to faithfully estimate the scale of missing components and infer plausible mappings on the missing pieces.

Our experimental results show that important attributes such as part symmetry and scale are well recovered by our system, suggesting that the network has learned the expected shape and form of the underlying class. We have shown (Figures 1, 2, 11, and 12) that our trained system generalizes well to unseen examples from the learned classes or from untrained but similar ones, and that the incorporation of prior knowledge benefits not only a complex

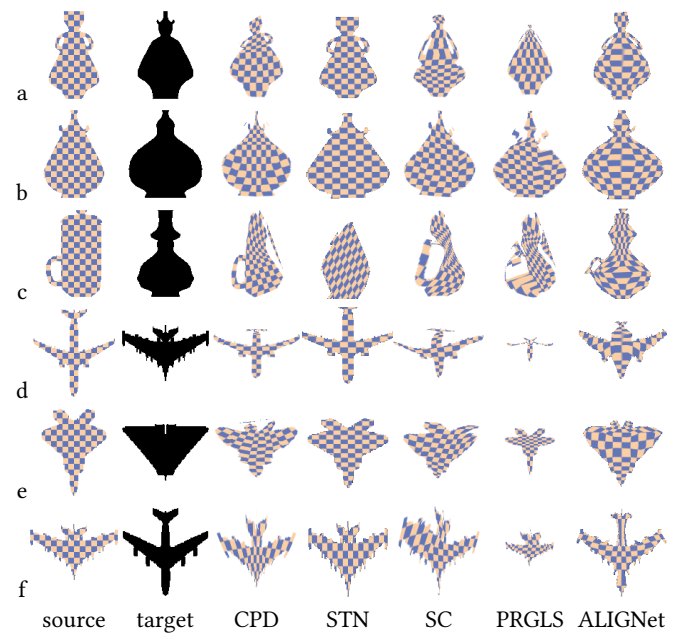


Fig. 23. Visual examples of complete shapes (no missing shape data). Test set results for: CPD [2010], STN [2015] (in ALIGNet framework), SC [2002], PRGLS [2016] and our method. The same set of parameters is used across all examples for ALIGNet and existing approaches.

setting where the target shape may be substantially partial, but also a simpler setting where the target shape is complete (Figure 23).

Looking forward, we suggest several directions for further research. While our current setting uses a simple loss function, it would be interesting to use more complex loss functions such as the perceptual loss [Johnson et al. 2016] or the earth-mover distance. Another possibility is to incorporate the *curriculum-learning* technique: first start with "easy" training examples (similar topologies and no missing parts), and as the network adapts to handle them, gradually include increasingly harder examples. Furthermore, extending the network scope to handle both partial source and target shapes is a challenging problem that may lead to a more generic solution. Our

warping grid is set to 8×8 for 2D shapes, and $7 \times 7 \times 7$ for 3D shapes. We deliberately opt for a milder degree of deformation, which inherently fosters smooth deformations. We note that to achieve a tighter alignment, it is possible to apply an ICP-based approach as a post-process. Finally, the incorporation of part awareness may potentially support a more semantic alignment, where advanced operations such as part addition and removal could help to maintain the structural integrity of the target shape.

7 ACKNOWLEDGEMENTS

We thank the anonymous reviewers for their helpful comments. This research was supported by the Israel Science Foundation as part of the ISF-NSFC joint program grant number (2217/15, 2472/17), and partially supported by ISF grant 2366/16. This research was partially supported by ERC-StG grant no. 757497 (SPADE).

REFERENCES

- Dror Aiger, Niloy J. Mitra, and Daniel Cohen-Or. 2008. 4pointss Congruent Sets for Robust Pairwise Surface Registration. In *ACM SIGGRAPH 2008 Papers (SIGGRAPH '08)*. ACM, New York, NY, USA, Article 85, 10 pages. <https://doi.org/10.1145/1399504.1360684>
- S. Belongie, J. Malik, and J. Puzicha. 2002. Shape matching and object recognition using shape contexts. *IEEE Transactions on Pattern Analysis and Machine Intelligence* 24, 4 (Apr 2002), 509–522.
- P. J. Besl and N. D. McKay. 1992. A method for registration of 3-D shapes. *IEEE Transactions on Pattern Analysis and Machine Intelligence* 14, 2 (Feb 1992), 239–256.
- Fred L. Bookstein. 1989. Principal warps: Thin-plate splines and the decomposition of deformations. *IEEE Transactions on pattern analysis and machine intelligence* 11, 6 (1989), 567–585.
- Angel X. Chang, Thomas Funkhouser, Leonidas Guibas, Pat Hanrahan, Qixing Huang, Zimo Li, Silvio Savarese, Manolis Savva, Shuran Song, Hao Su, Jianxiong Xiao, Li Yi, and Fisher Yu. 2015. *ShapeNet: An Information-Rich 3D Model Repository*. Technical Report arXiv:1512.03012 [cs.GR]. Stanford University — Princeton University — Toyota Technological Institute at Chicago.
- Christopher B Choy, JunYoung Gwak, Silvio Savarese, and Manmohan Chandraker. 2016. Universal correspondence network. In *Advances in Neural Information Processing Systems*. 2414–2422.
- Alexey Dosovitskiy, Philipp Fischer, Eddy Ilg, Philip Hausser, Caner Hazirbas, Vladimir Golkov, Patrick van der Smagt, Daniel Cremers, and Thomas Brox. 2015. FlowNet: Learning Optical Flow with Convolutional Networks. In *Proceedings of the 2015 IEEE International Conference on Computer Vision (ICCV) (ICCV '15)*. IEEE Computer Society, Washington, DC, USA, 2758–2766. <https://doi.org/10.1109/ICCV.2015.316>
- Martin A Fischler and Robert C Bolles. 1981. Random sample consensus: a paradigm for model fitting with applications to image analysis and automated cartography. *Commun. ACM* 24, 6 (1981), 381–395.
- Ravi Garg, Vijay Kumar BG, Gustavo Carneiro, and Ian Reid. 2016. Unsupervised cnn for single view depth estimation: Geometry to the rescue. In *European Conference on Computer Vision*. Springer, 740–756.
- Max Jaderberg, Karen Simonyan, Andrew Zisserman, and Koray Kavukcuoglu. 2015. Spatial Transformer Networks. In *Proceedings of the 28th International Conference on Neural Information Processing Systems (NIPS'15)*. MIT Press, Cambridge, MA, USA, 2017–2025.
- B. Jian and B. C. Vemuri. 2011. Robust Point Set Registration Using Gaussian Mixture Models. *IEEE Transactions on Pattern Analysis and Machine Intelligence* 33, 8 (Aug 2011), 1633–1645.
- Justin Johnson, Alexandre Alahi, and Li Fei-Fei. 2016. Perceptual losses for real-time style transfer and super-resolution. In *European Conference on Computer Vision*. Springer, 694–711.
- Angjoo Kanazawa, David W Jacobs, and Manmohan Chandraker. 2016. WarpNet: Weakly supervised matching for single-view reconstruction. In *Proceedings of the IEEE Conference on Computer Vision and Pattern Recognition*. 3253–3261.
- Longin Jan Latecki and Rolf Lakamper. 2000. Shape similarity measure based on correspondence of visual parts. *IEEE Transactions on Pattern Analysis and Machine Intelligence* 22, 10 (2000), 1185–1190.
- Jun Li, Yongjun Chen, Lei Cai, Ian Davidson, and Shuiwang Ji. 2017. Dense Transformer Networks. *arXiv preprint arXiv:1705.08881* (2017).
- Haibin Ling and David W Jacobs. 2007. Shape classification using the inner-distance. *IEEE transactions on pattern analysis and machine intelligence* 29, 2 (2007), 286–299.
- Or Litany, Emanuele Rodolà, Alex M Bronstein, and Michael M Bronstein. 2017. Fully spectral partial shape matching. In *Computer Graphics Forum*, Vol. 36. Wiley Online Library, 247–258.
- Jiayi Ma, Ji Zhao, Jinwen Tian, Alan L Yuille, and Zhuowen Tu. 2014. Robust point matching via vector field consensus. *IEEE Transactions on Image Processing* 23, 4 (2014), 1706–1721.
- Jiayi Ma, Ji Zhao, and Alan L Yuille. 2016. Non-rigid point set registration by preserving global and local structures. *IEEE Transactions on Image Processing* 25, 1 (2016), 53–64.
- G. Mori and J. Malik. 2003. Recognizing objects in adversarial clutter: breaking a visual CAPTCHA. In *2003 IEEE Computer Society Conference on Computer Vision and Pattern Recognition, 2003. Proceedings*, Vol. 1. I-134–I-141 vol.1.
- A. Myronenko and X. Song. 2010. Point Set Registration: Coherent Point Drift. *IEEE Transactions on Pattern Analysis and Machine Intelligence* 32, 12 (Dec 2010), 2262–2275.
- S. Rusinkiewicz and M. Levoy. 2001. Efficient variants of the ICP algorithm. In *Proceedings Third International Conference on 3-D Digital Imaging and Modeling*. 145–152.
- Thomas W Sederberg and Scott R Parry. 1986. Free-form deformation of solid geometric models. *ACM SIGGRAPH computer graphics* 20, 4 (Aug 1986), 151–160.
- Amit Shaked and Lior Wolf. 2016. Improved Stereo Matching with Constant Highway Networks and Reflective Confidence Learning. *arXiv preprint arXiv:1701.00165* (2016).
- Edgar Simo-Serra, Eduard Trulls, Luis Ferraz, Iasonas Kokkinos, Pascal Fua, and Francesc Moreno-Noguer. 2015. Discriminative learning of deep convolutional feature point descriptors. In *Proceedings of the IEEE International Conference on Computer Vision*. 118–126.
- Ayush Tewari, Michael Zollhöfer, Hyeongwoo Kim, Pablo Garrido, Florian Bernard, Patrick Perez, and Christian Theobalt. 2017. Mofa: Model-based deep convolutional face autoencoder for unsupervised monocular reconstruction. In *The IEEE International Conference on Computer Vision (ICCV)*, Vol. 2.
- A. Thayananthan, B. Stenger, P. H. S. Torr, and R. Cipolla. 2003. Shape Context and Chamfer Matching in Cluttered Scenes. In *Proceedings of the 2003 IEEE Computer Society Conference on Computer Vision and Pattern Recognition (CVPR'03)*. IEEE Computer Society, Washington, DC, USA, 127–133.
- Bin Fan, Yurun Tian, and Fuchao Wu. 2017. L2-Net: Deep learning of discriminative patch descriptor in euclidean space. In *Conference on Computer Vision and Pattern Recognition (CVPR)*.
- Yanghai Tsai and Takeo Kanade. 2004. *A Correlation-Based Approach to Robust Point Set Registration*. Springer Berlin Heidelberg, Berlin, Heidelberg, 558–569.
- Yunhai Wang, Shmulik Asafi, Oliver van Kaick, Hao Zhang, Daniel Cohen-Or, and Baoguan Chen. 2012. Active co-analysis of a set of shapes. *ACM Transactions on Graphics (TOG)* 31, 6 (2012), 165.
- M Ersin Yumer and Niloy J. Mitra. 2016. Learning semantic deformation flows with 3d convolutional networks. In *European Conference on Computer Vision*. Springer, 294–311.
- Jure Zbontar and Yann LeCun. 2016. Stereo matching by training a convolutional neural network to compare image patches. *Journal of Machine Learning Research* 17, 1–32 (2016), 2.
- Andy Zeng, Shuran Song, Matthias Nießner, Matthew Fisher, Jianxiong Xiao, and Thomas Funkhouser. 2017. 3DMatch: Learning Local Geometric Descriptors from RGB-D Reconstructions. In *CVPR*.
- Yefeng Zheng and D. Doermann. 2006. Robust point matching for nonrigid shapes by preserving local neighborhood structures. *IEEE Transactions on Pattern Analysis and Machine Intelligence* 28, 4 (April 2006), 643–649.